Institut für Theoretische Physik

Bachelorarbeit

zum Thema

Investigation of the fermion sign problem in graphene at finite charge density

Autor: Arndt Henning Ziegler

Prüfer: Prof. Dr. Lorenz von Smekal

Zweitprüfer: Dr. Dominik Smith

Abgabedatum: 30. September 2016

Abstract

The aim of this Bachelor's thesis is to determine the range of values that the chemical potential at various Coulomb interaction strengths can take as a parameter of a grand-canonical description of monolayer graphene at fixed temperature without causing a fermion sign problem which makes Monte-Carlo-simulations unfeasible. The focus is on Coulomb interaction energies varying from zero to full vacuum interaction strength and chemical potentials varying from zero to 1.0 and in addition from 2.5 to 2.9 eV to study the sign problem at the neck-disrupting Lifshitz transition in graphene.

Kurzfassung

Das Ziel dieser Bachelorarbeit ist das Vorzeichenproblem, welches ein Hindernis bei der Anwendung von Monte-Carlo-Simulationen darstellt, in Graphen bei fester Temperatur zu untersuchen, wenn ein Tight-Binding Hamiltonian plus Coulombwechselwirkung und chemisches Potential für die großkanonsiche Beschreibung verwendet wird. Variable Größen sind dabei die Wechselwirkungsstärke, welche von 10 Prozent bis 100 Prozent der Vakuumwechselwirkungsstärke variiert wird, und das chemische Potential, welches von 0,1 bis 1,0 und 2,5 bis 2,9 eV aufgedreht wird. Letzterer Bereich soll untersucht werden, um den neck-disrupting Lifshitzübergang bei 2.7 eV abzudecken.

Contents

1 Introduction

Graphene started out as a purely theoretical construct, which was considered not to exist in nature because of its thermodynamical instability, as shown by Landau [1] in 1937 and others. However, later on, beginning in the 60s of the 20th century, experimentalists were able to produce graphene, like Boehm et al in 1962 [2]. The discrepancy between experiment and theory could later be resolved by the argument, that one has to consider crumpling into the 3rd dimension of the graphene sheet [3]. First systematic examinations of the electronic properties of graphene were conducted in 2005 by Novoselov et al [4], which were rewarded with the nobel prize in physics in 2010. For further information on the properties of graphene see [5] and references therein.
From a theoretical viewpoint, one wishes to find suitable models for graphene to calculate and reproduce the experimental data. For a history of modeling and calculation methods used, see [7]. In short, graphene is modeled by a tight-binding Hamiltonian plus Coulomb interaction of the electrons, with which the partition function and other observables can be calculated using Hybrid-Monte-Carlo simulation (in the remaining called 'HMCs' for notational convenience). Recently a chemical potential has been introduced to study graphene beyond half-filling. That is, the Fermi surface can be moved and the states populated at absolute zero temperature altered. This way van-Hove-singularities in the bandstructure (see 2.1) can be reached and examined, resulting in a topological phase transition called neck disrupting Lifshitz transition [8]. Regarding experiments, the Fermi surface can be changed by doping or an applied electric field [5]
Because there are other interesting phenomena such as superconductivity possible in graphene (see for example [6]), one wishes to do further calculations at variable chemical potential. But there is a problem coming with the introduction of a chemical potential, called fermion sign problem which can make HMCs unfeasible. More on that in section 2.4. The purpose of this thesis is therefore to investigate the range of values the chemical potential can take at various Coulomb interaction strengths without the sign problem being so severe that HMCs cease to be feasible.

2 Theoretical Basics

2.1 Graphene

Graphene is an allotrope of carbon consisting of atoms arranged on a hexagonal lattice in two dimensions. The lattice can be described by 3 vectors in a manner employed in solid state physics, namely by dividing the lattice in two sublattices, each of them having the same basis, which are connected by a third vector pointing from any atom on the one lattice to the corresponding atom on the other lattice that is displaced in the direction of this vector, see the 6x4 lattice depicted in figure 1. The pink axes show the direction of the basis vectors and the blue dots and red dots representing atoms on sublattice one and sublattice two, respectively. The indexing scheme is straight-forward, first the atoms of the first sublattice are counted, the enumeration is then continued on the other sublattice.

The bandstructure of graphene was derived in [8] using tight-binding approach, stating

$$E(k_x, k_y) = \pm t\sqrt{3 + 4\cos(\frac{\sqrt{3}a}{2}k_x)\cos(\frac{3a}{2}k_y) + 2\cos(\sqrt{3}ak_x)} \qquad (1)$$

where k_x and k_y are the components of the wave vector and t is the hopping parameter, describing the interaction between nearest neighboring sites in the tight-binding model. See figure 2 for a visualization of the bandstructure.
In that figure one can see one of the interesting phenomena mentioned in the introduction are the dirac cones in the bandstructure. These are the areas in the wavenumer space where the upper and lower bands meet. Electrons with those wave vectors are governed by the dirac equation, that is, they behave

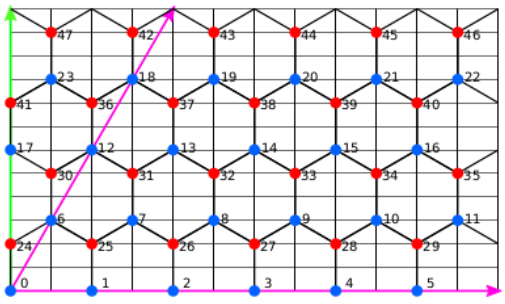

Figure 1: The graphene lattice with basis vectors and indexing scheme. Excerpt from [7]

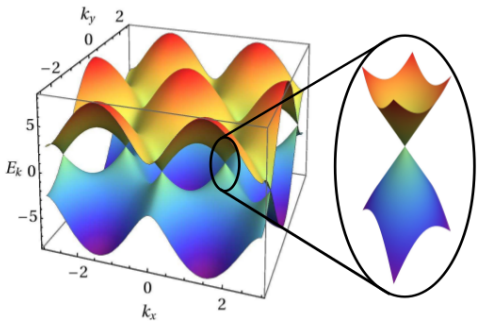

Figure 2: Visualization of the bandstructure in tight-binding graphene. Excerpt from [8]

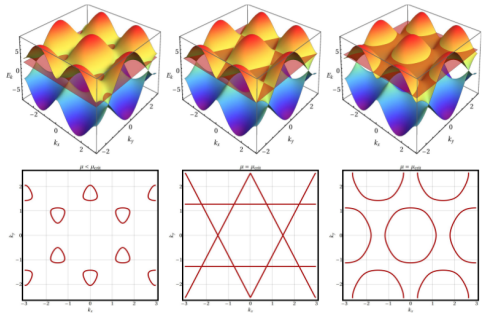

Figure 3: Visualization of the Fermi surface at various chemical potentials. Excerpt from [8]

like relativistic particles. Furthermore, the density of states vanishes at the dirac cones [8].
In figure 3 the topology of the Fermi surface at various chemical potentials is depicted. When the Fermi surface reached the level of a van Hove singularity in the density of states, its topology changes. This happens at chemical potential $\mu = 2,7\text{eV}$ [8]. Further phenomena are associated with this topological phase transition, see section 6.

2.2 Hamiltonian

After this little introduction about graphene the Hamiltonian describing electrons in graphene will be presented. As mentioned before, tight-binding approach with Coulomb interaction chemical potential is used and the Hamiltonian is expressed in second quantization. The same Hamiltonian was used in [8]. The tight-binding term is

$$H_{tb} = t \sum_{x,ynn,s} (a^\dagger_{x,s} a_{y,s} + a^\dagger_{y,s} a_{x,s}) \tag{2}$$

where nn denotes summation only over nearest neighbors, t ist the hopping parameter and $a^\dagger_{x,s}$ and $a_{x,s}$ creation and annihilation operators of an electron with spin s at site x.
The term accounting for the Coulomb interaction is

$$H_{Coul} = \frac{1}{2} \sum_{x,y,s} q_x V_{xy} q_y \tag{3}$$

with the charge operator $q_x = a^\dagger_{x,1} a_{x,1} + a^\dagger_{x,-1} a_{x,-1} - 1$ and the Coulomb interaction matrix V_{xy}. Minus one was added to the charge operators to make the system neutral at half-filling. Exploiting the commutation relation for fermions, the charge operator can be rewritten: $q_x = a^\dagger_{x,1} a_{x,1} - a_{x,-1} a^\dagger_{x,-1}$.
Chemical potential is added to the system via the following term

$$H_{chem} = -\mu \sum_{x,s} a^\dagger_{x,s} a_{x,s} \tag{4}$$

Furthermore, there is an additional term used for technical purposes

$$H_m = \sum_x m_s (a^\dagger_{x,1} a_{x,1} + a^\dagger_{x,-1} a_{x,-1}) \tag{5}$$

where m_s is one for one sublattice, and minus one for the other, therefore breaking sublattice symmetry.
In conclusion, the resulting Hamiltonian is

$$\begin{aligned} H =& t \sum_{x,ynn,s} (a^\dagger_{x,s} a_{y,s} + a^\dagger_{y,s} a_{x,s}) - \mu \sum_{x,s} a^\dagger_{x,s} a_{x,s} \\ &+ m_s \sum_x (a^\dagger_{x,1} a_{x,1} + a^\dagger_{x,-1} a_{x,-1}) + \frac{1}{2} \sum_{x,y,s} q_x V_{xy} q_y \end{aligned} \tag{6}$$

2.3 Partition function

In the following the path integral formulation of the partition function of graphene will be derived, repeating the steps in [7] with additional chemical potential. Only the important steps are included here, an extensive version can be found there. The goal is to arrive eventually at a formulation that is suitable to perform HMCs.
First, to eliminate summation over the spin components, hole creation and annihilation operators are introduced to replace spin down annihilation and creation operators, respectively. That is,

$$\begin{aligned} a^\dagger_{x,-1} &\to b_x \\ a_{x,-1} &\to b^\dagger_x \\ a^\dagger_{x,1} &\to a^\dagger_x \\ a_{x,1} &\to a_x \end{aligned} \tag{7}$$

Moreover, on one lattice the sign of the hole operators is flipped, meaning $b_x \to -b_x$ and $b^\dagger_x \to -b^\dagger_x$. Now the Hamiltonian expressed with hole operators in normal order is

$$\begin{aligned} H =& t \sum_{x,ynn} (a^\dagger_x a_y + a^\dagger_y a_x + b^\dagger_x b_y + b^\dagger_y b_x) - \mu \sum_{x,s} a^\dagger_x a_x - b^\dagger_x b_x \\ &+ m_s \sum_x (a^\dagger_x a_x + b^\dagger_x b_x) + \frac{1}{2} \sum_{x,y,s} q_x V_{xy} q_y \end{aligned} \tag{8}$$

The purpose of this manipulation is to be able to formulate the partition function using coherent states, which are constructed like this

$$|\phi, \eta\rangle = \exp(-\sum_x \phi_x a^\dagger_x + \eta_x b^\dagger_x) \, |0\rangle \tag{9}$$

with ϕ_x and η_y being the associated Grassmannumbers to each creation operator [9] and $|0\rangle$ the vacuum state of the Fock space. After slicing $e^{-\beta H}$ into $e^{(-\delta H)^{N_t}}$, with $\delta = \beta / N_t$, which is later interpreted as computer time for the molecular dynamics evolution, the partition function $\operatorname{Tr} e^{-\beta H}$ can be written using coherent states and anti-periodic boundary conditions:

$$\begin{aligned} \operatorname{Tr} e^{-\beta H} =& \int \prod_{t=0}^{N_t} (\prod_x d\phi^*_{x,t} d\phi_{x,t} d\eta^*_{x,t} d\eta_{x,t}) \\ &\times \exp(\sum_x \phi^*_{x,t} \phi_{x,t} + \eta^*_{x,t} \eta_{x,t}) \, \langle \phi_{t+1}, \eta_{t+1}| \, e^{-\delta H} \, |\phi_t, \eta_t\rangle \end{aligned} \tag{10}$$

Evaluation the matrix elements yields by using the abbreviation $D\phi = \prod_{t=0}^{N_t} \prod_x d\phi_{x,t}$

$$\begin{aligned}
\operatorname{Tr} e^{-\beta H} = \int D\phi D\phi^* D\eta D\eta^* \exp[-\delta(& \underbrace{\frac{1}{2}\sum_{x,y} Q_{x,t+1,t} V_{x,y} Q_{y,t+1,t}}_{\text{Coulomb interaction}} \\
& \underbrace{+ \frac{1}{2}\sum_x V_{x,x}(\phi^*_{x,t+1}\phi_{x,t} + \eta^*_{x,t+1}\eta_{x,t})}_{\text{Coulomb diagonal elements}} \\
& \underbrace{- t \sum_{x,ynn} \phi^*_{x,t+1}\phi_{y,t} + \eta^*_{x,t+1}\eta_{y,t} + \phi^*_{y,t+1}\phi_{x,t} + \eta^*_{y,t+1}\eta_{x,t}}_{\text{Tight-binding}} \\
& \underbrace{+ \sum_x m_s(\phi^*_{x,t+1}\phi_{x,t} + \eta^*_{x,t+1}\eta_{x,t})}_{\text{staggered mass}} \\
& \underbrace{- \mu \sum_x \phi^*_{x,t+1}\phi_{x,t} - \eta^*_{x,t+1}\eta_{x,t})}_{\text{chemical potential}} \\
& \underbrace{- \sum_x \phi^*_{x,t+1}(\phi_{x,t+1} - \phi_{x,t}) + \eta^*_{x,t+1}(\eta_{x,t+1} - \eta_{x,t})]}_{\text{weighting function and scalar product}} \qquad (11)
\end{aligned}$$

where $Q_{x,t,t'} = \phi^*_{x,t}\phi_{x,t'} - \eta^*_{x,t}\eta_{x,t'}$.
To get rid of the fourth powers in the Coulomb interaction term, a Hubbard-Stratonovich-transformation is performed:

$$\begin{aligned}
& \exp(-\frac{\delta}{2}\sum_{x,y} Q_{x,t+1,t} V_{x,y} Q_{y,t+1,t}) \propto \\
& \int D\psi \exp(\frac{\delta}{2}\sum_{t=0}^{N_t-1}\sum_{x,y} \psi_{x,t} V^{-1}_{x,y} \psi_{y,t} - i\delta \sum_{t=0}^{N_t-1}\sum_x \psi_{x,t} Q_{x,t+1,t}) \qquad (12)
\end{aligned}$$

yielding

$$\begin{aligned}\mathrm{Tr}\, e^{-\beta H} = \int D\phi D\phi^* D\eta D\eta^* D\psi \exp[-\delta \sum_{t=0}^{N_t-1} (\\ \underbrace{\frac{1}{2}\sum_{x,y}\psi_{x,t}V^{-1}_{x,y}\psi_{y,t} - i\sum_{t=0}^{N_t-1}\sum_{x}\psi_{x,t}Q_{x,t+1,t}}_{\text{Transformation}} \\ \underbrace{+\frac{1}{2}\sum_{x}V_{x,x}(\phi^*_{x,t+1}\phi_{x,t} + \eta^*_{x,t+1}\eta_{x,t})}_{\text{Coulomb diagonal elements}} \\ \underbrace{-t\sum_{x,ynn}\phi^*_{x,t+1}\phi_{y,t} + \eta^*_{x,t+1}\eta_{y,t} + \phi^*_{y,t+1}\phi_{x,t} + \eta^*_{y,t+1}\eta_{x,t}}_{\text{Tight-binding}} \\ \underbrace{+\sum_{x} m_s(\phi^*_{x,t+1}\phi_{x,t} + \eta^*_{x,t+1}\eta_{x,t})}_{\text{staggered mass}} \\ \underbrace{-\mu\sum_{x}\phi^*_{x,t+1}\phi_{x,t} - \eta^*_{x,t+1}\eta_{x,t})}_{\text{chemical potential}} \\ \underbrace{-\sum_{t=0}^{N_t-1}\sum_{x}\phi^*_{x,t+1}(\phi_{x,t+1}-\phi_{x,t}) + \eta^*_{x,t+1}(\eta_{x,t+1}-\eta_{x,t})]}_{\text{weighting function and scalar product}} \end{aligned} \tag{13}$$

The last step is to introduce a matrix

$$\begin{aligned}M_{x,y,t,t'}(\mu) =& \delta_{x,y}(\delta_{t,t'} - \delta_{t-1,t'}) - t\frac{\beta}{N_t}\sum_{nn}\delta_{y,x}\delta_{t-1,t'} + m_s\frac{\beta}{N_t}\delta_{x,y}\delta_{t-1,t'} \\ &+ \frac{V_{x,y}\beta}{2N_t}\delta_{x,y}\delta t-1,t' + i\psi_{x,t}\frac{\beta}{N_t}\delta_{x,y}\delta_{t-1,t'} - \mu\frac{\beta}{N_t}\delta_{x,y}\delta_{t-1,t'} \end{aligned} \tag{14}$$

where nn denoting, that s takes every neighboring value at fixed y. The partition function can now be expressed by this matrix

$$\begin{aligned}\mathrm{Tr}\, e^{-\beta H} = \int D\phi D\phi^* D\eta D\eta^* D\psi \exp(-\frac{\delta}{2}\sum_{t=0}^{N_t-1}\sum_{x,y}\psi_{x,t}V^{-1}_{x,y}\psi_{y,t} \\ - \sum_{t,t'}^{N_t-1}\sum_{x,x'}\phi^*_{x,t}M_{x,x',t,t'}(\mu)\phi^*_{x',t'} + \eta^*_{x,t}M^*_{x,x',t,t'}(-\mu)\eta^*_{x',t'}) \end{aligned} \tag{15}$$

Notice that in the last term, the matrix is evaluated with a flipped sign of the chemical potential. This is the very cause of the sign problem, as expanded on in the next section. By carrying out the Gaussian integral

$$\int (\prod_{m=1}^{n} d\chi_m^* d\chi_m) \exp(-\sum_{i,j=1}^{n} \chi_i^* A_{i,j} \chi_j) \propto \det A \tag{16}$$

the final form is obtained

$$\mathrm{Tr}\, e^{-\beta H} = \int D\psi \det M(\mu) \det M^*(-\mu) \exp(-\frac{\delta}{2} \sum_{t=0}^{N_t-1} \sum_{x,y} \psi_{x,t} V_{x,y}^{-1} \psi_{y,t}) \tag{17}$$

2.4 Reweighting

To be able to evaluate an integral with HMCs, it has to be of the following form

$$I = \int D\phi P(\phi) O(\phi) \tag{18}$$

where P denotes the weight of the integral and O the observable. P has to be real and positive in order to be interpreted as a probability distribution by HMCs. But Equation 17 does not satisfy this condition, for the determinants can be complex numbers in general. If they were of the form $\det M(\mu) \det M^*(\mu) = |detM(\mu)|^2$, no problem would occur, since the result would be real and positive. To this end eq. 17 is rewritten, like demonstrated in [13] for QCD:

$$\begin{aligned} Z &= \int D\psi \det M(\mu) \det M^*(-\mu) \frac{\det M^*(\mu)}{\det M^*(\mu)} \exp(-\frac{\delta}{2} \sum_{t=0}^{N_t-1} \sum_{x,y} \psi_{x,t} V_{x,y}^{-1} \psi_{y,t}) \\ &= \int D\psi |\det M(\mu)|^2 \exp(-\frac{\delta}{2} \sum_{t=0}^{N_t-1} \sum_{x,y} \psi_{x,t} V_{x,y}^{-1} \psi_{y,t}) \frac{\det M^*(-\mu)}{\det M^*(\mu)} \end{aligned} \tag{19}$$

Using eq. 19, one has to evaluate the following integral in order to calculate an observable O:

$$\begin{aligned}\mathrm{Tr}(e^{-\beta H}O) &= \frac{1}{Z}\int D\psi \det M(\mu) \det M^*(-\mu)\frac{\det M^*(\mu)}{\det M^*(\mu)} \\ &\quad \times \exp(-\frac{\delta}{2}\sum_{t=0}^{N_t-1}\sum_{x,y}\psi_{x,t}V^{-1}_{x,y}\psi_{y,t})O(\phi) \\ &= \frac{1}{Z}\int D\psi \underbrace{|\det M(\mu)|^2 \exp(-\frac{\delta}{2}\sum_{t=0}^{N_t-1}\sum_{x,y}\psi_{x,t}V^{-1}_{x,y}\psi_{y,t})}_{\mathrm{P}} \\ &\quad \times \underbrace{\frac{\det M^*(-\mu)}{\det M^*(\mu)}O(\phi)}_{\mathrm{O'}} \end{aligned} \tag{20}$$

While interpreting the factor referred to as O' as new observable, eq. 20 assumes a form that can be evaluated by HMCs.
Remark: In [8] it was assumed that $\det M^*(-\mu) = \det M^*(\mu)$ by flipping the sign of the chemical potential for holes, since the bandstructure in the nearest-neighbor tight-binding model is symmetric under spin-flip.
The problem now is that the ratio of determinants, as a complex number possessing both a magnitude and a phase, could be highly oscillatory, meaning the phase would be uniformly distributed over the complex unit circle and thus yielding zero as mean value, making Monte-Carlo-simulations unfeasible. That is called the sign problem and the very topic of this thesis.

3 Hybrid Monte Carlo algorithm

In this section the basics of the Hybrid Monte Carlo algorithm used in this thesis will be presented. Main source is [10].

3.1 Basic Monte-Carlo

Monte Carlo Simulations are mainly used to calculate high-dimensional integrals because of their probabilistic approach as opposed to deterministic algorithms, which lowers the run time of the algorithm.
Consider an integral of a function $f(x)$ over a volume V. The integral can then be approximated by

$$\int_V f(x)dx \approx \frac{V}{N}\sum_{i=1}^{N} f(x_i) \tag{21}$$

with x_i being N randomly picked points of the volume. As N grows to infinity, the approximation converges to the exact value of the integral, as assured by the law of large numbers.

3.2 Importance Sampling

Most of the time, a non-random distribution of the points is more efficient. For example, if a Gaussian distribution is to be integrated over the set of real numbers, most points would not contribute much to the value of the integral, if the Gaussian distribution function is evaluated at those points. Instead the points are selected following a Gaussian distribution by themselves, meaning points at the center are preferred. So if $p(x)$ is the normalized distribution according to which the points are picked, the integral is approximated like

$$\int_V f(x)dx \approx \frac{V}{N}\sum_{i=1}^{N} \frac{f(x_i)}{p(x_i)} \tag{22}$$

To determine the distribution the reweighted formulation of the partition function follows, eq. 19 is rewritten using eq. 16:

$$
\begin{aligned}
Z &= \int D\psi |\det M(\mu)|^2 \exp(-\frac{\delta}{2}\sum_{t=0}^{N_t-1}\sum_{x,y}\psi_{x,t}V^{-1}_{x,y}\psi_{y,t})\frac{\det M^*(-\mu)}{\det M^*(\mu)} \\
&= \int D\psi D\chi D\chi^* \exp(-\underbrace{\frac{\delta}{2}\sum_{t=0}^{N_t-1}\sum_{x,y}\psi_{x,t}V^{-1}_{x,y}\psi_{y,t}}_{\mathrm{S}(\psi)} \\
&\quad - \underbrace{\sum_{t',t=0}^{N_t-1}\sum_{x,y}\chi^*_{x,t}(MM^\dagger)^{-1}_{x,x',t,t'}\chi_{x',t'}}_{\mathrm{S'}(\chi)})\frac{\det M^*(-\mu)}{\det M^*(\mu)}
\end{aligned}
\tag{23}
$$

So $p(\psi,\chi) = \exp(-S(\psi) - S'(\chi))$. The points for χ are selected simply by following the distribution given by $\exp(-S'(\chi))$. Another expression for 'selecting points' is 'generating field', since ψ and χ are interpreted as fields.

3.3 Molecular dynamics

The ψ-field is generated using a Markov chain molecular dynamics evolution, meaning that a trajectory in fictitious time through the phase space is calculated based on the field Hamiltonian and a corresponding fictitious momentum field [7]. The equation of motion defined by this Hamiltonian is solved by discretizing and using a leapfrog integrator. Since there are discretization errors (step-size errors), a metropolis acceptance test is performed afterwards, which rejects any configuration that is not a valid phase space point at given energy.
Thermalization and correlation of the configurations are two problems one has to pay attention to when performing the molecular dynamics evolution. They are discussed in the next section.

4 Simulations

Simulations were conducted to calculate the reweighted partition function 23 with the ratio of determinants as an effective observable at $\beta = 2.0$ eV^{-1} on a 6x6 lattice with $N_t = 12$ and the chemical potential ranging from $\mu = 0.1$ to $\mu = 1.0$ and $\mu = 2.5$ to $\mu = 2.9$ eV with a stepsize of 0.1 eV at Coulomb interaction strengths of 10, 20, 40, 80 and 100 percent of vacuum strength. The staggered mass is set to zero. At every combination of chemical potential and Coulomb interaction strength 1500 measurements were made with two updates of the molecular dynamics trajectory in between every measurement. As leapfrog integrator steps number 1000 was set and as step size 0.3 unless otherwise indicated in the results section. There are a few possible technical issues to be considered to guarantee the integrity of the calculations.

4.1 Thermalization

Thermalization is the process of a system reaching thermodynamical equilibrium. The graphene lattice has to be in equilibrium associated with a specific energy for the measurements to make sense. Eventually reaching equilibrium is ensured by the acceptance test, accepting configurations in equilibrium with a much higher probability, but it is not clear how long it takes to get there from a arbitrary starting configuration. An indicator for equilibrium is the variation of the Hamiltonian. If it fluctuates around a static mean value, equilibrium is reached.
The measurements exhibited almost instant thermalization throughout the entire range of parameters, so there is no further consideration necessary.

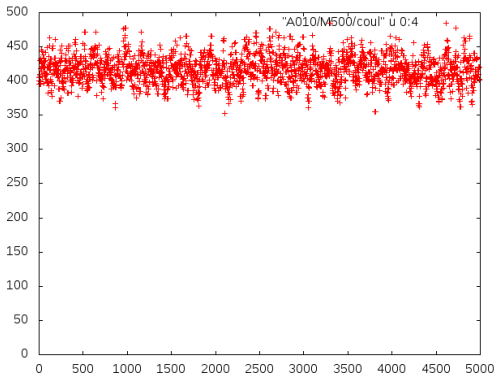

Figure 4: Thermalization at 10% Coulomb interaction strength and $\mu = 0.5$ eV

4.2 Correlation

Another problem is the correlation of configurations in the phase space by the simple fact that the trajectory has a finite step size and cannot reach every other point from a given point in phase space in one step. So the next point depends not only one the previous one, but also several ones prior to that. One method to solve this problem is using the binning-method as described in [8]. In this thesis however, it is assumed that enough updates are made throughout the measurements that correlations cease to be of significant impact on the data.

4.3 Technical data

The simulations were performed on nVidia graphic boards of the type 'GeForce GTX 980 Ti'. For further information, see [18].
The source code of the program developed by Smith and von Smekal [7] was modified to calculate the ratio of determinants 23, compiled and run on a computer cluster using the graphic boards mentioned above at Justus-Liebig-Universitaet Gießen in August 2016.

5 Results

In this section, the results of the simulations are presented. In general, the observable is a complex number, but the magnitude turned out to be almost constant in every measurement, with a average fluctuation of under 10 percent. Thus it can be considered constant and can be absorbed in the measure of the integral, yielding complex numbers limited to the complex unit circle, that is, numbers with magnitude one. Therefore the only interesting parts of the measurements are the phases of the complex numbers and will be displayed as histograms in the following.
The histograms were made with gnuplot.

5.1 Mu = 0.1 - 1.0

The plots were superpositioned with a Gaussian fit to make it easier to compare the dispersion at different parameters, measured by the root mean square deviation. At every Coulomb interaction strength the distribution of the phases are practically even at a chemical potential of $\mu = 0.5$ eV and greater and are therefore not included. That means the sign problem is severe at those chemical potentials.

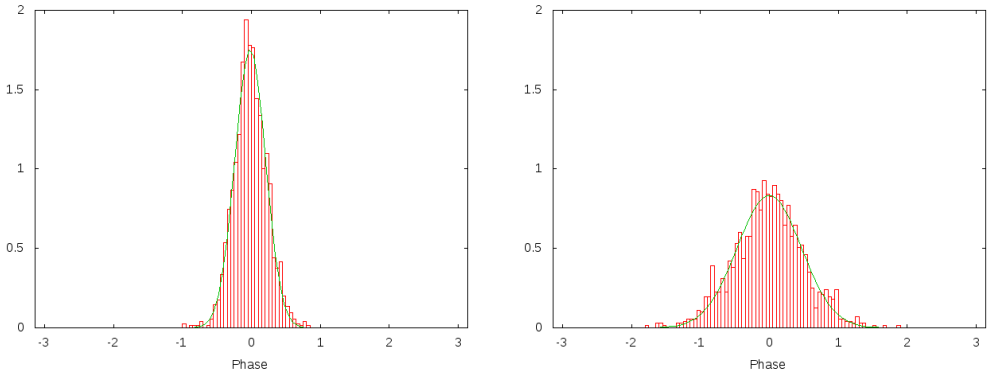

(a) $\mu = 0.1$ eV

(b) $\mu = 0.2$ eV

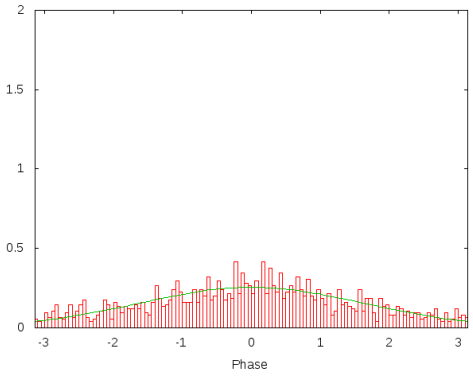

(c) $\mu = 0.3$ eV

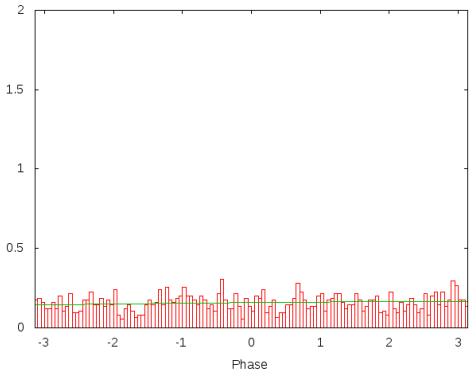

(d) $\mu = 0.4$ eV

Figure 5: Phase distribution at 10% Coulomb interaction strength

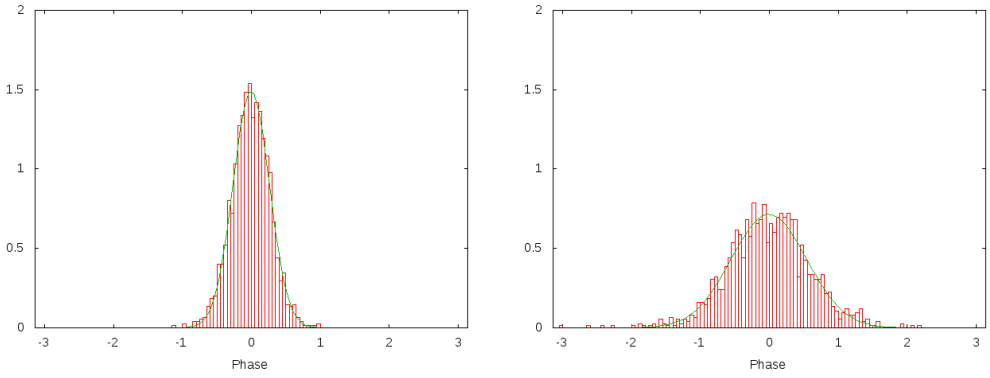

(a) $\mu = 0.1$ eV

(b) $\mu = 0.2$ eV

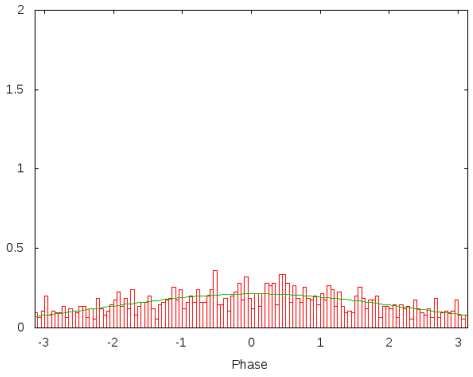

(c) $\mu = 0.3$ eV

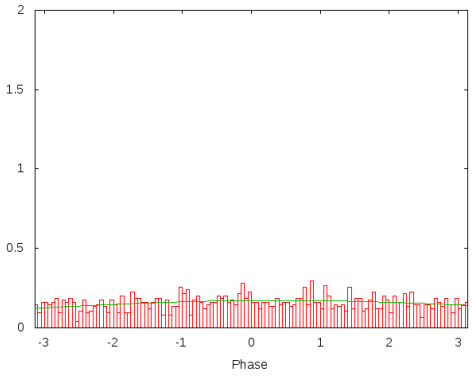

(d) $\mu = 0.4$ eV

Figure 6: Phase distribution at 20% Coulomb interaction strength

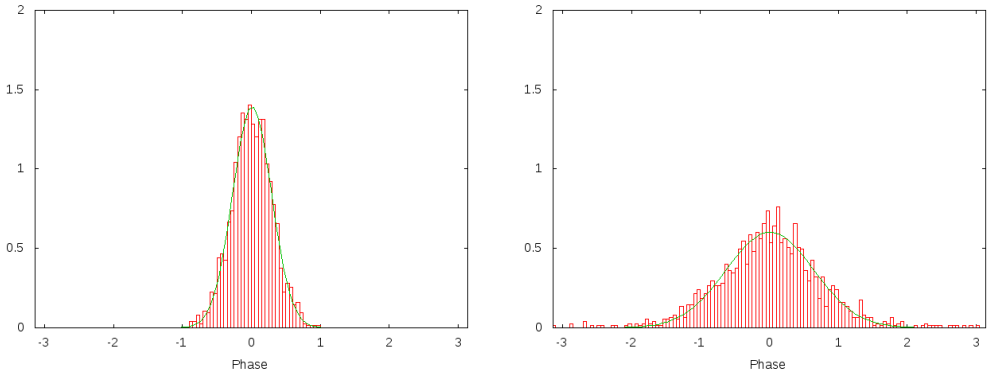

(a) $\mu = 0.1$ eV

(b) $\mu = 0.2$ eV

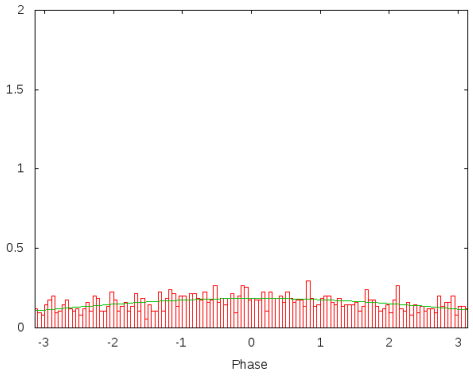

(c) $\mu = 0.3$ eV

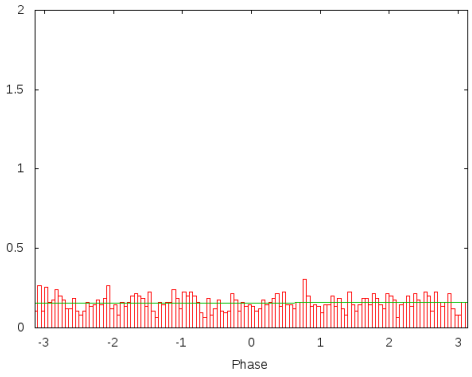

(d) $\mu = 0.4$ eV

Figure 7: Phase distribution at 40% Coulomb interaction strength

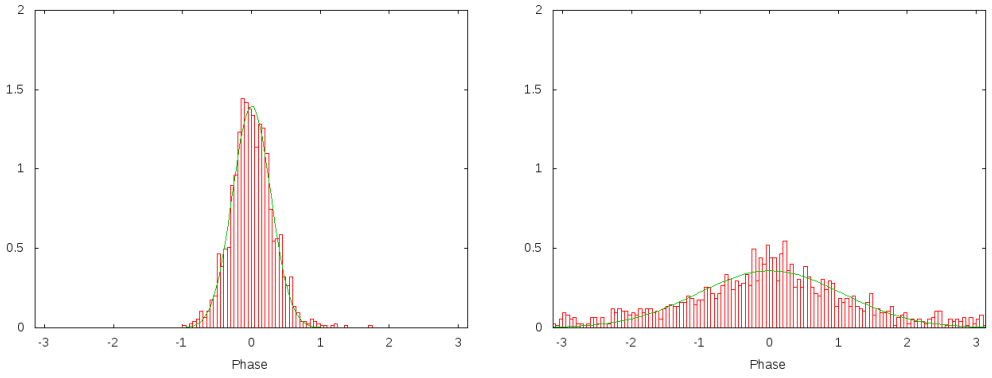

(a) $\mu = 0.1$ eV

(b) $\mu = 0.2$ eV

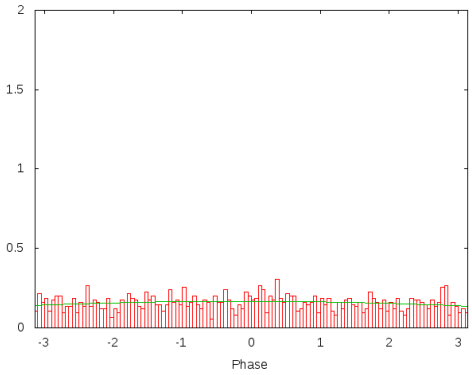

(c) $\mu = 0.3$ eV

Figure 8: Phase distribution at 80% Coulomb interaction strength

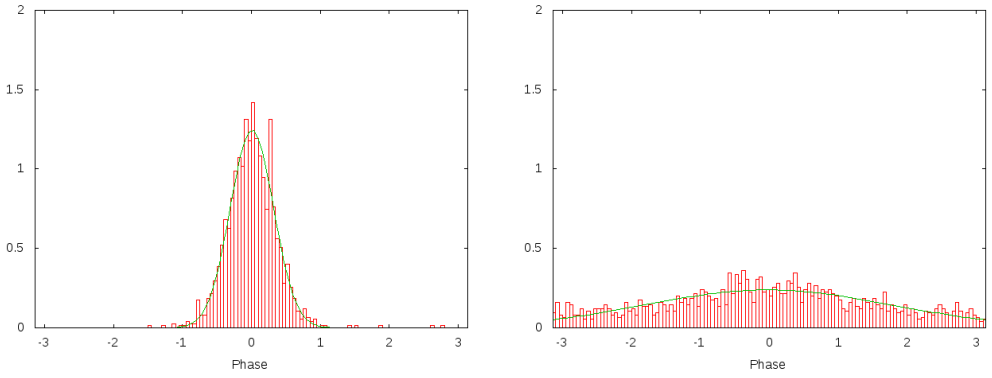

(a) $\mu = 0.1$ eV

(b) $\mu = 0.2$ eV

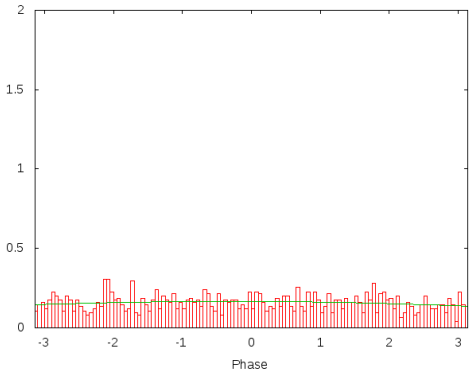

(c) $\mu = 0.3$ eV

Figure 9: Phase distribution at 100% Coulomb interaction strength

To compare the results at different parameters quantitatively, the root mean square deviation of every plot is listed in the table below. The sort sequence is designed to make the comparison between different Coulomb interaction strengths easier. All values are rounded to 2 decimal positions. Mean and root mean square values are practically dimensionless, because the phase is expressed in radial measure. The format of the first column is ' - percentage of Coulomb interaction strength in vacuum used - , - chemical potential in eV - '.

Parameters	RMS	Mean
10%, 0.1	0.22	-0.02
20%, 0.1	0.26	0.00
40%, 0.1	0.28	0.01
80%, 0.1	0.28	0.00
100%, 0.1	0.31	0.01
10%, 0.2	0.47	0.00
20%, 0.2	0.55	0.00
40%, 0.2	0.63	0.00
80%, 0.2	1.05	0.01
100%, 0.2	1.78	-0.01
10%, 0.3	1.63	0.00
20%, 0.3	2.17	0.05
40%, 0.3	3.08	0.07
80%, 0.3	5.12	-0.14
100%, 0.3	5.48	-0.30
10%, 0.4	12.4	3.60
20%, 0.4	4.31	0.40
40%, 0.4	71.2	13.9
80%, 0.4	-	-
100%, 0.4	-	-

Two main outcomes are evident. First, at a chemical potential of $\mu = 0.4$ the Gaussian fit ceases to make sense because of great root mean square deviation and means that are out of range. When compared to figure 6d the Gaussian fit algorithm even seems to fail at 20% Coulomb interaction strength because the visual examination yields no sufficient evidence for a concentration of the phase as suggested by the relatively low root mean square value. Therefore, combined with the observation mentioned above, the sign problem is severe at chemical potential $\mu = 0.4$ eV and greater.
Second, root mean square deviation raises when Coulomb interaction strength

increases. That is, the phase distribution flattens out at higher energy and the sign problem becomes stronger.

5.2 Mu = 2.5 - 2.9

The sign problem at chemical potential ranging from $\mu = 2.5$ to $\mu = 2.9$ was studied to determine the feasibility of HMCs at this range, where the neck-disrupting Lifshitz transition and other phenomena happen. For every set of parameters 1000 measurements were conducted as opposed to 1500 for the parameters studied in the last section. The simulations yielded the following results.
At Coulomb interaction strengths of 10% and 20% almost every measurement yielded zero as result not only for the phase of the integral, but also for magnitude, real part and imaginary part. A few measurements stated the phase as numerical π while real and imaginary part remained zero. Because of the fact that the phase is calculated using real and imaginary part, these results are considered to be due to a predetermined variable within the program or simply as an systematic error. Measurements were conducted a second time with altered Leapfrog integrator parameters, because the zero results could be caused by an instability in the integrator. The step number was set to 100,000 and the step size to 0.003 to remain a product of 300, which turned out to be optimal during the simulations conducted in [8]. But the results were still zero without change in the number of numerical pis. This could be due to the single precision complex variables that were used. Further studies should use double precision to determine the origin of this result.
At 40% Coulomb interaction strength 8% on average of the measurements resulted in a finite phase, the remaining ones in zero or an infinite magnitude, meaning that the range the complex variables could handle was exceeded. A second conduction with altered Leapfrog integrator parameters as above yielded no increase in the percentage of finite phases. The little data that were of use showed an distribution with no significant concentration. Figure 10a and 10b show an example. The higher the Coulomb interaction strength the more finite phases were obtained, ranging from 1% at 10% strength and 24% at 100% strength.

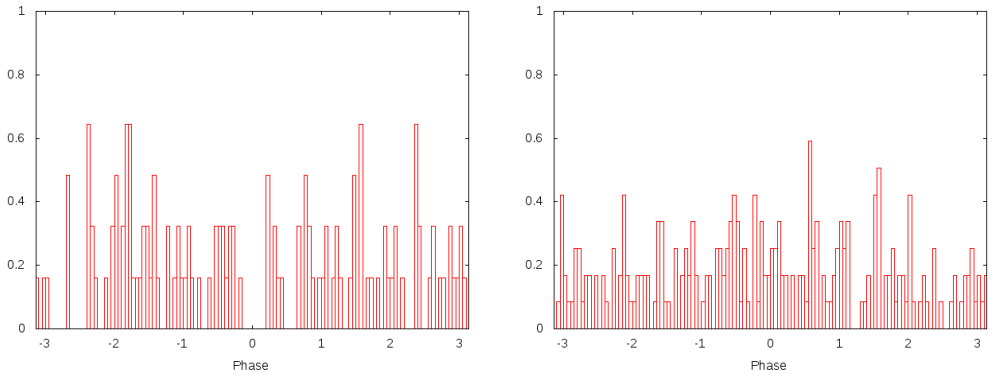

(a) $\mu = 2.8$ eV (b) $\mu = 2.9$ eV

Figure 10: Phase distribution at 40% Coulomb interaction strength

At 80% and 100% Coulomb interaction strength 96% and 92% of the measurements were finite, respectively. But as at previous Coulomb interaction strengths no concentration in the phase distribution are evident. The results at 80% Coulomb interaction strength are included below, the ones at 100% do not deviate significantly from them.
Apparently the sign problem is severe at chemical potential ranging from $\mu = 2.5$ and $\mu = 2.9$ eV, making HMCs unfeasible.

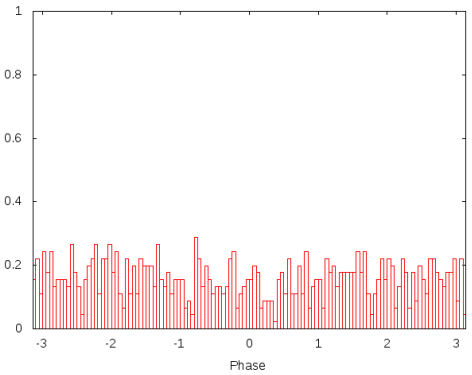

(a) $\mu = 2.5$ eV

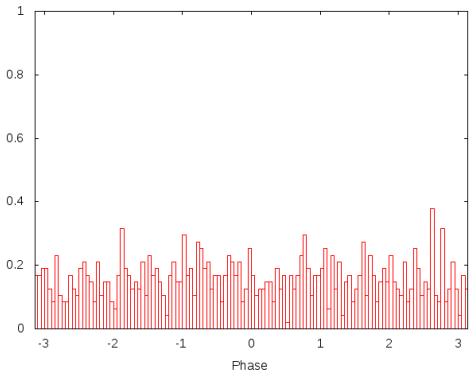

(b) $\mu = 2.6$ eV

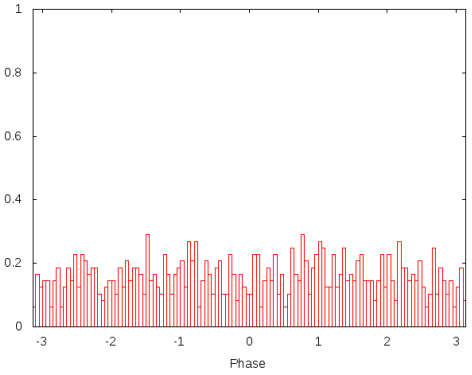

(c) $\mu = 2.7$ eV

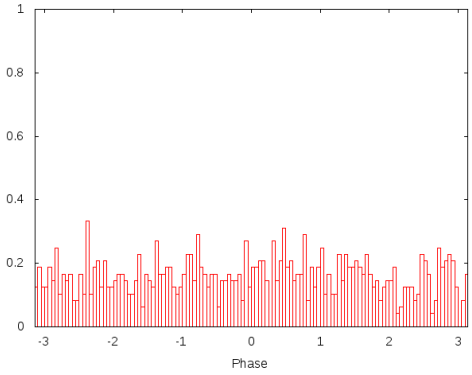

(d) $\mu = 2.8$ eV

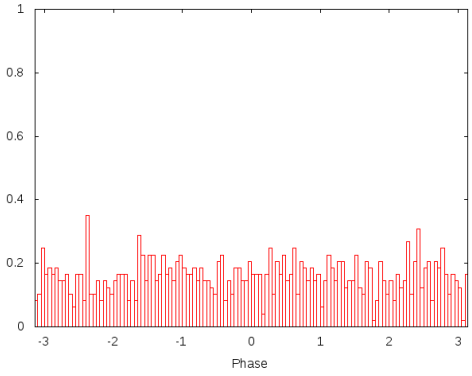

(e) $\mu = 2.9$ eV

Figure 11: Phase distribution at 80% Coulomb interaction strength

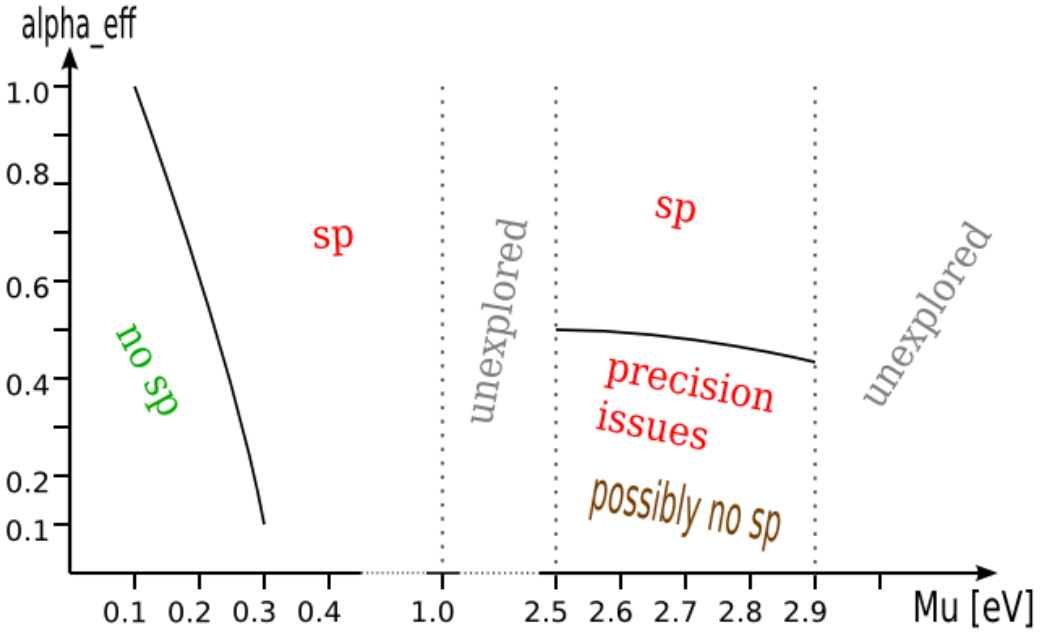

Figure 12: α_{eff} to μ diagram on the simulation results. Extrapolations were made to provide continuous lines. Abbreviations used: 'sp' : sign problem occurs in this area, ' no sp' : sign problem does not occur in this area. Made with inscape

6 Conclusion and outlook

In summary, the simulations conducted for this thesis showed the following results (see figure 12 for a visual summary).
At chemical potential $\mu = 0.4$ eV and greater, the sign problem in tight binding graphene with Coulomb interaction is severe regardless of Coulomb interaction strength. More precisely, at 10% interaction strength HMCs are still feasible up to $\mu = 0.3$ eV, but this limit drops steadily as interaction strength increases down to $\mu = 0.1$ eV at full interaction strength. Beyond those limits, the sign problem impedes the use of HMCs.
Around the Lifshitz transition at $\mu = 2.7$ eV, the precision used by the simulations is not good enough to yield results at 40% interaction strength and below. Possibly the sign problem is sufficiently non-severe to yield a concentration in the phase distribution at very weak Coulomb interactions. On the other hand, the sign problem is indeed severe at 80% interaction strength and greater.
A continuation and expansion of this thesis should definitely include measurements at the Lifshitz transition with a higher precision, so that this

region can be clarified. Furthermore the tight binding Hamiltonian could be expanded in a way that it includes next-nearest neighbor hopping, which makes the model better and more realistic. This new Hamiltonian is subject to a sign problem as well, even without a chemical potential, because the two sublattices get intertwined by the next-nearest hopping term.
The region around the Lifshitz transition is of particular interest for further research, because it is rich in interesting phenomena, as already mentioned in the introduction. With Angle resolved photoemission studies [17] one can examine the van Hove singularity in the bandstructure of doped graphene and can thus investigate the region of the Lifshitz transition experimentally. Interesting phenomena include quantum hall effect [16], d-wave superconductivity [15] and other exotic ground states.

References

[1] L. D. Landau *Zur Theorie der Phasenumwandlungen* II. Phys. Z. Sowjetunion 11, 26–35, 1937

[2] H. P. Boehm, A. Clauss, G. O. Fischer, *Dünnste Kohlenstoff-Folien*, Zeitschrift fue Naturforschung, 17 b, 150 – 153, 1962

[3] J. C. Meyer, A. K. Geim, M. I. Katsneslon, K. S. Novoselov, T. J. Booth, S. Roth, *The structure of suspended graphene sheets*, Nature 446, 60-63, March 2007

[4] K. S. Novoselov, D. Jiang, F. Schedin, T. J. Booth, V. V. Khotkevich, S. V. Morozov, A. K. Geim, *Two-dimensional atomic crystals*, Proceedings of the National Academy of Sciences of the United States of America 102, 30, 10451-10453, 2005

[5] A. H. Castro Neto, F. Guinea, N. M. R. Peres, K. S. Novoselov, A. K. Geim, *The electronic properties of graphene*, Review of Modern Physics, **81**, 109, 2009

[6] Chapman, J., et al. *Superconductivity in Ca-doped graphene*, arXiv:1508.06931 (2015).

[7] D. Smith and L. von Smekal, *Monte Carlo simulation of the tight-binding model of graphene with partially screened Coulomb interactions* `http://arxiv.org/pdf/1403.3620v1.pdf`

[8] Michael Körner *Master's thesis: Investigation of topological phase transitions in graphene by Monte Carlo simulations*

[9] J. W. Negele and H. Orland, *Quantum Many-Particle Systems*, Westview Press 1998

[10] Bernd A. Berg *Markov chain monte carlo simulations and their statistical analysis*, World Scientific Publishing, 2004

[11] S. Duane, A. D. Kennedy, B. J. Pendleton and D. Roweth, Phys. Lett. B **195**, 216 (1987)

[12] R. C. Brower, C. Rebbi and D. Schaich, *Hybrid Monte Carlo Simulation of Graphene on the Hexagonal Lattice* `http://arxiv.org/pdf/1101.5131v1.pdf`

[13] Masanori Hanada, Yoshinori Matsuo and Naoki Yamamoto, *Sign problem and phase quenching in finite-density QCD: models, holography, and lattice* https://arxiv.org/pdf/1205.1030v3.pdf

[14] Jacob Friedrich Finkenrath, *Stochastic Methods for the Fermion Determinant in Lattice Quantum Chromodynamics* http://elpub.bib.uni-wuppertal.de/servlets/DerivateServlet/Derivate-4620/dc1502.pdf

[15] J. Vucicevic et al, *d-wave superconductivity on the honeycomb bilayer*, Physical Review B **86**, 214505 (2012)

[16] Tao Li *Spontaneous quantum hall effect in quarter-doped Hubbard model on honeycomb lattice and its possible realization in quarter-doped graphene system*, Europhysics Letters 97.3 (2012): 37001

[17] A. Damascelli et al *Angle resolved photoemission studies of the cuprate superconductivity* Rev. Mod. Phys. **75** 473, 2003

[18] nVidia-corporation *Information on GeForce GTX 980 Ti*, http://www.geforce.com/hardware/desktop-gpus/geforce-gtx-980-ti, 09/22/2016

Selbstständigkeitserklärung

Hiermit versichere ich, die vorgelegte Thesis selbstständig und ohne unerlaubte fremde Hilfe und nur mit den Hilfen angefertigt zu haben, die ich in der Thesis angegeben habe. Alle Textstellen, die wörtlich oder sinngemäß aus veröffentlichten Schriften entnommen sind, und alle Angaben die auf mündlichen Auskünften beruhen, sind als solche kenntlich gemacht. Bei den von mir durchgeführten und in der Thesis erwähnten Untersuchungen habe ich die Grundsätze guter wissenschaftlicher Praxis, wie sie in der ‚Satzung der Justus-Liebig-Universität zur Sicherung guter wissenschaftlicher Praxis' niedergelegt sind, eingehalten. Gemäß § 25 Abs. 6 der Allgemeinen Bestimmungen für modularisierte Studiengänge dulde ich eine Überprüfung der Thesis mittels Anti-Plagiatssoftware.

30.09.2016
Datum

A.H. Ziegler
Unterschrift